



## Effects of co-precipitation temperature on structure and properties of La and Y doped cerium zirconium mixed oxides

Lian-jie ZHANG<sup>1,2</sup>, Mei-sheng CUI<sup>1,2,3,4</sup>, Hao WANG<sup>1,2,3</sup>, Yong-ke HOU<sup>1,2,3</sup>,  
Shi-lei CHEN<sup>1,2</sup>, Zhi-zhe ZHAI<sup>1,3</sup>, Zhi-qi LONG<sup>1,2,3,4</sup>, Yong-qi ZHANG<sup>1,2,3,4</sup>

1. National Engineering Research Center for Rare Earth, GRINM Group Co., Ltd., Beijing 100088, China;
2. General Research Institute for Nonferrous Metals, Beijing 100088, China;
3. GRIREM Advanced Materials Co., Ltd., Beijing 100088, China;
4. GRIREM Hi-Tech Co., Ltd., Langfang 065201, China

Received 9 March 2021; accepted 28 September 2021

**Abstract:** Due to the oxygen storage and release properties, cerium zirconium mixed oxides are recognized as the key material in automotive three-way catalysts. To reveal the effects of co-precipitation temperature on structure, physical and chemical properties of multi-doped cerium zirconium mixed oxides, a series of La and Y doped cerium zirconium mixed oxides (CZLYs) were synthesized via a co-precipitation method, and the physical and chemical properties of CZLYs were systemically characterized by XRD, N<sub>2</sub> adsorption–desorption, TEM, XPS, oxygen storage capacity (OSC) and hydrogen temperature programmed reduction (H<sub>2</sub>-TPR). The results show that co-precipitation temperature is an important parameter to influence the crystal size, oxygen storage capacity and thermal stability of CZLYs. When the co-precipitation temperature was 60 °C, the best redox properties and thermal stability of CZLYs were obtained. After thermal treatment at 1100 °C for 10 h, the specific surface area and oxygen storage capacity of the corresponding aged sample were 15.42 m<sup>2</sup>/g and 497.7 μmol/g, respectively. In addition, a mechanism was proposed to reveal the effects of co-precipitation temperature on the structure and properties of CZLYs.

**Key words:** La and Y doping; cerium zirconium mixed oxides; co-precipitation temperature; crystal size; thermal stability

## 1 Introduction

Nowadays, much attention has been paid to reducing the automobile exhaust because of the serious air pollution. To abate the air pollution, the automotive emission standards have been continuously tightening [1], and the three-way catalyst is used for the automobile exhaust purification. As the key washcoat material of automotive catalyst, cerium zirconium mixed oxides (CZs) can effectively improve the catalytic performance of catalysts because of their unique

physical and chemical properties [2,3]. However, the performance of pure cerium zirconium mixed oxides deteriorates due to the particle sintering under high working temperature. Therefore, it has been a great challenge to improve the thermal stability and redox performance of CZs for many years.

Compared to sol–gel, hydrothermal, micro-emulsion, and template methods, co-precipitation method has been widely used to prepare CZs in industry because it is controllable and easy to operate [4–9]. Concluding from Refs. [10–15], the structure and properties of CZs prepared by

co-precipitation method are influenced by preparation conditions, including types of raw materials, addition of complexing agents, speed of solution feeding, stirring intensity, pH of co-precipitation, temperature of the co-precipitation reaction, and so on. Co-precipitation temperature is undoubtedly a key factor because it has significant impact on the viscosity and supersaturation, the reaction rate, and the reaction equilibrium. Previous research [15–17] showed that, during the process of co-precipitation, an appropriate co-precipitation temperature promoted the growth of crystal grains and the formation of high crystallinity precipitates, which led to high thermal stability of the prepared material. CUI et al [15] also investigated the effects of co-precipitation temperature on CZs in reverse feeding method. With the increase of co-precipitation temperature, the growth of crystal grains was promoted and the redox and oxygen storage capacity (OSC) performances were enhanced. In addition, the modification of rare earth elements is an effective approach to improve the thermal stability of CZs, and much attention has been paid to rare earth elements doped CZs. Thus, the effects of the co-precipitation temperature on the nano/multi-doped CZs remain to be clarified, as the precipitation behavior of doping elements would be influenced by the precipitation temperature, which would further affect the physical and chemical properties of rare earth elements doped CZs.

Considering that the co-precipitation temperature is an important parameter to influence the properties of RE-doped CZs, therefore, in this work, a series CZLYs were prepared at different co-precipitation temperatures via co-precipitation method. The chemical and physical properties of the obtained CZLYs were characterized by X-ray diffraction (XRD),  $N_2$  adsorption–desorption, transmission electron microscope (TEM), X-ray photoelectron spectroscopy (XPS), oxygen storage capacity (OSC) and hydrogen temperature programmed reduction ( $H_2$ -TPR), and the effects of co-precipitation temperature on the structure, thermal stability and redox properties of CZLYs were studied systematically. At last, a mechanism was proposed to reveal the effects of co-precipitation temperature on the structure and properties of CZLYs.

## 2 Experimental

### 2.1 Materials preparation

All CZs were prepared by a co-precipitation method. To prepare the precursor of CZLYs (molar ratio of Ce/Zr/(La+Y) being 33:57:10), the ammonia solution was added dropwise to the mixed solution of  $Ce(NH_4)_2(NO_3)_6$ ,  $ZrO(NO_3)_2$ ,  $La(NO_3)_3$  and  $Y(NO_3)_3$  at different co-precipitation temperatures of 20, 40, 60 and 80 °C, respectively. After washing, the obtained precipitates were dried overnight at 60 °C, and the dried samples were marked as CZLY-*X*-d (*X*=20, 40, 60, 80) where *X* stands for the co-precipitation temperature. Then, the fresh samples were obtained by calcining the dried samples at 800 °C for 3 h. Fresh samples prepared at different co-precipitation temperatures were marked as CZLY-*X*-f (*X*=20, 40, 60, 80). The fresh samples were further calcined at 1100 °C for 10 h, and the corresponding aged samples were obtained and marked as CZLY-*X*-a (*X*=20, 40, 60, 80).

### 2.2 Characterization techniques

The phase structures of fresh and aged samples were analyzed by an X'Pert PRO MRD diffractometer equipped with a  $Cu K_\alpha$  radiation source ( $\lambda=0.15418$  nm). The samples were measured at a step size of  $0.02^\circ$  in the  $2\theta$  range of  $10^\circ$  to  $90^\circ$  and the working voltage and current of the instrument were 40 kV and 25 mA, respectively. The microscopic morphology and structure of the samples were observed using a Tecnai G2 F20 transmission electron microscope with an accelerating voltage of 200 kV. XPS measurements were carried out on a ESCALAB 250Xi photoelectron spectrometer equipped with a monochromatic  $Al K_\alpha$  radiation source. The step size of XPS measurements was 0.05 eV, and the electron binding energy value of each element was calibrated with the standard C 1s (284.8 eV).

The specific surface area and pore size distribution of the samples were analyzed by a Quadrasorb SI-KR/4MP automatic specific surface area and pore size analyzer at  $-196^\circ C$ , and the samples were degassed at 280 °C for 3 h before testing. The OSC and  $H_2$ -TPR of the samples were tested by a Chembet PULSAR TPR/TPD chemical adsorption instrument. For the OSC test, 10 vol.%

H<sub>2</sub>/Ar was first introduced to reduce the samples at 800 °C for 1 h, and then O<sub>2</sub> pulse titration was used at 500 °C to calculate the OSC value of the samples. For the H<sub>2</sub>-TPR test, the samples were first oxidized by 5 vol.% O<sub>2</sub>/Ar at 500 °C for 1 h, after that the gas was switched to helium until the temperature dropped below 30 °C, and then 10 vol.% H<sub>2</sub>/Ar was input for H<sub>2</sub>-TPR. The temperature was increased to 950 °C at a rate of 5 °C/min.

### 3 Results and discussion

#### 3.1 Crystal structure

Figure 1(a) shows the XRD patterns of CZLY-*X*-f (*X*=20, 40, 60, 80). In Fig. 1(a), all CZLY-*X*-f (*X*=20, 40, 60, 80) have four obvious diffraction peaks, in which  $2\theta$  centered at around 29.4°, 34.1°, 49.0° and 58.1°, indexing to the (111), (200), (220) and (311) planes of Ce<sub>0.5</sub>Zr<sub>0.5</sub>O<sub>2</sub> (ICDD PDF No. 04-005-9597, cubic phase), respectively. Clearly, the peak positions of all samples are similar,

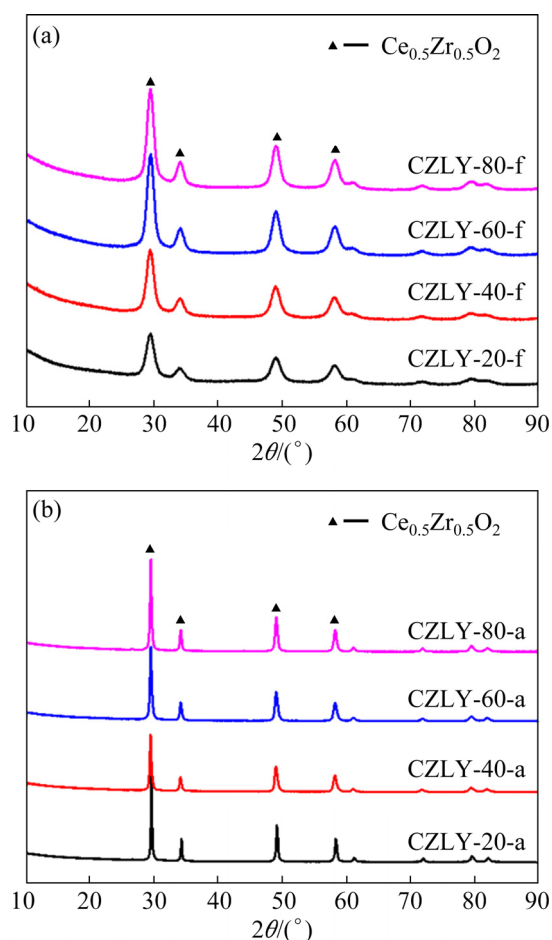


**Fig. 1** XRD patterns of CZLY-*X*-f (*X*=20, 40, 60, 80) (a) and CZLY-*X*-a (*X*=20, 40, 60, 80) (b)

which means that the crystal structure is not altered when the co-precipitation temperature is changed. The diffraction peaks of CZLY-20-f are broader than those of other samples, indicating that it has smaller crystal size and lower crystallinity. With the increase of co-precipitation temperature, the diffraction peaks of fresh samples become narrower, which means that the crystal size and crystallinity are enlarged and improved, respectively [18]. Figure 1(b) shows the XRD patterns of CZLY-*X*-a (*X*=20, 40, 60, 80). Compared with the fresh samples, the positions and symmetry of main diffraction peaks of CZLY-*X*-a (*X*=20, 40, 60, 80) are basically unchanged without new diffraction peaks, which indicates that no phase separation occurs after thermal treatment. However, the diffraction peaks become sharper after thermal treatment, revealing that the size of crystal grains becomes larger. It should be noted that the intensity of diffraction peak of CZLY-20-a and CZLY-80-a is stronger than those of the other two samples. The results show that CZLY-20-a and CZLY-80-a have larger crystal sizes.

Table 1 shows the structural parameters of CZLY-*X*-f and CZLY-*X*-a (*X*=20, 40, 60, 80) calculated according to the Scherrer formula and Bragg equation. It can be observed that the (111) crystal plane spacing of all samples is around 0.303 nm. With increasing the co-precipitation temperature, the crystal size of CZLY-*X*-f (*X*=20, 40, 60, 80) increases from 6.1 to 7.3 nm. After thermal treatment, the grain growth of all samples occurred to some degree. In particular, CZLY-20-f

**Table 1** Structural parameters of CZLY-*X*-f and CZLY-*X*-a (*X*=20, 40, 60, 80)

Sample	$2\theta/(\circ)$	(111) crystal plane spacing/nm	Crystal size/nm	$\Delta D/\%$
CZLY-20-f	29.42	0.304	6.1	–
CZLY-40-f	29.40	0.304	6.8	–
CZLY-60-f	29.43	0.303	7.1	–
CZLY-80-f	29.42	0.304	7.3	–
CZLY-20-a	29.48	0.303	51.3	741
CZLY-40-a	29.42	0.304	38.2	462
CZLY-60-a	29.45	0.303	37.3	425
CZLY-80-a	29.45	0.303	49.5	578

$\Delta D$  represents the increment rate of crystal size after thermal treatment at 1100 °C for 10 h

was sintered seriously after treatment at 1100 °C for 10 h, with the largest crystal size of 51.3 nm in aged samples. Clearly, CZLY-60-f shows the best thermal stability, with the smallest crystal size (37.3 nm) and smallest  $\Delta D$  (425%) of aged samples. Thus, it can be concluded that the thermal stability of CZLY- $X$ -f ( $X=20, 40, 60$ ) can be improved by appropriately increasing the co-precipitation temperature. However, the thermal stability of CZLY-80-a decreased again, with a large  $\Delta D$  of 578%, which is higher than 425% of CZLY-60-a. This implies that excessive co-precipitation temperature has negative effect on the thermal stability of CZLYs [15].

The HRTEM images of CZLY- $X$ -f ( $X=20, 40, 60, 80$ ) are listed in Fig. 2. As seen from Fig. 2, the interplane spacings of all samples are approximately 0.310 nm, which can be indexed to the (111) plane of the  $\text{Ce}_{0.5}\text{Zr}_{0.5}\text{O}_2$  (ICDD PDF No. 04-005-9597), agreeing with the interplane spacings calculated by XRD results.

### 3.2 Surficial chemical environment

The surficial chemical environment of samples was further analyzed by X-ray photoelectron spectroscopy. It can be seen that the Ce 3d XPS spectrum can be deconvoluted to eight peaks (Fig. 3(a)). The peaks located at  $u$  (901.0–901.4 eV),  $u'$  (904.0–904.3 eV),  $u''$  (907.4–907.7 eV) and  $u'''$  (916.7–916.9 eV) are related to Ce 3d<sub>3/2</sub>, and the peaks labeled  $v$  (882.5–882.8 eV),  $v'$  (885.5–885.8 eV),  $v''$  (889.0–889.3 eV) and  $v'''$  (898.3–898.6 eV) correspond to Ce 3d<sub>5/2</sub> [19,20]. The bands labeled  $u'$  and  $v'$  represent the Ce<sup>3+</sup> species, while the other peaks represent the Ce<sup>4+</sup> species. The proportion of Ce<sup>3+</sup> on the surface can be calculated by the peak area ratio of  $(u' + v') / (u + u' + u'' + u''' + v + v' + v'' + v''')$  [21], and the results are listed in Table 2. The O 1s XPS peaks for fresh samples are shown in Fig. 3(b), the two bands at 531.6–532.0 and 529.6–530.1 eV represent the chemisorbed oxygen ( $\text{O}_{\text{ads}}$ ) and lattice oxygen ( $\text{O}_{\text{latt}}$ ), respectively [22].

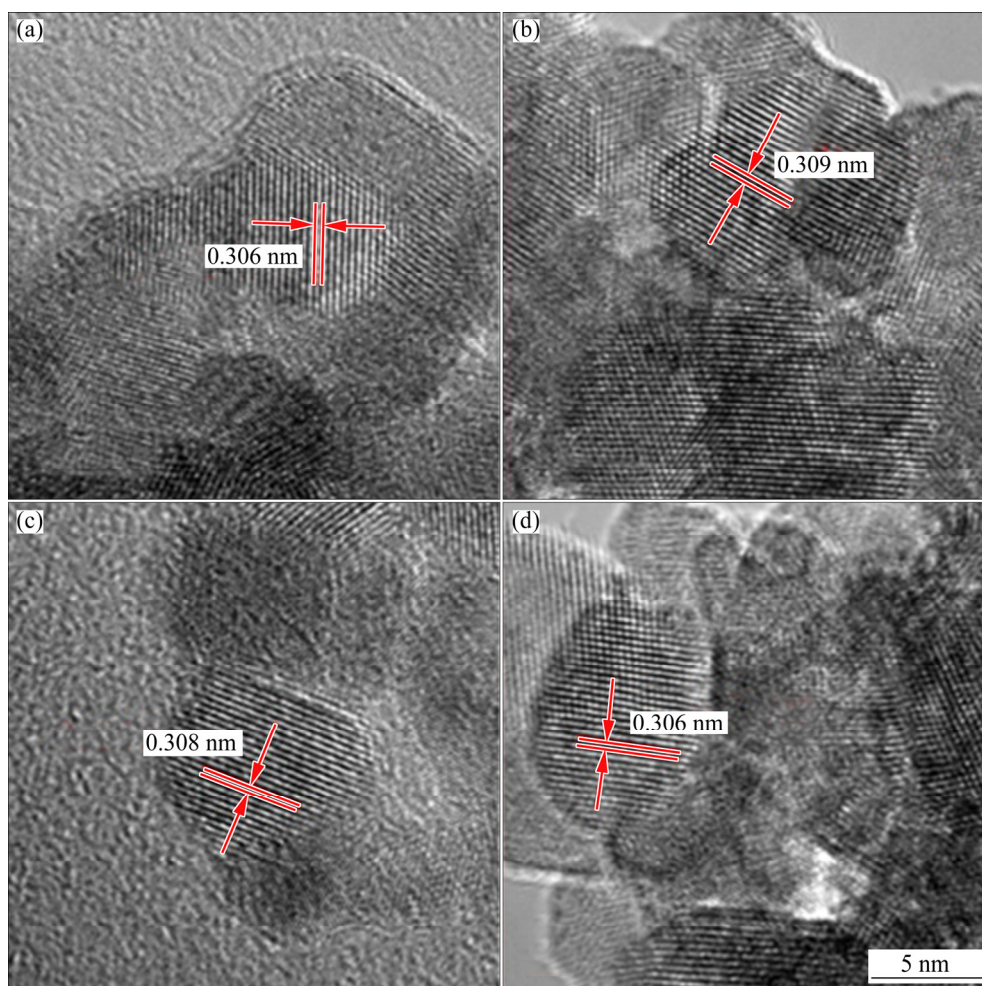


Fig. 2 HRTEM images of CZLY-20-f (a), CZLY-40-f (b), CZLY-60-f (c), and CZLY-80-f (d)

Table 2 shows the surficial element compositions and molar ratios of the CZLY-*X*-f and CZLY-*X*-a (*X*=20, 40, 60, 80). For CZLY-20-f, the surficial compositions of Ce, Zr and La+Y elements are 29.610%, 55.850% and 14.540%, respectively. With the increase of co-precipitation temperature, the surficial element composition shows no obvious change. However, the surface molar ratio of Ce<sup>3+</sup> shows an increase trend for fresh samples from 0.226 (CZLY-20-f) to 0.258 (CZLY-60-f). More Ce<sup>3+</sup> in CZLY-60-f would endow it with more defects, which is beneficial to the improvement of redox performance. On the contrary, the surface element contents of CZLYs have been changed significantly after thermal treatment. Generally, the content of Ce element on the surface decreased, while the contents of La and Y elements increased after thermal treatment. Especially for CZLY-20-f, the surface content of Ce decreased from 29.610% to 17.992%, and the content of La + Y elements increased from 14.540% to 28.529%. These mean that thermal treatment would lead to the surface

element rearrangement, with the Ce element migrating from the surface to the bulk and the enrichment of La and Y elements on the surface. And the severe element rearrangement of CZLY-20-a results in inhomogeneous distribution of elements. Among aged samples, the surface composition of CZLY-60-a had the minimal change which benefited from its homogeneous distribution of elements and structural stability. Furthermore, the Ce<sup>3+</sup> and adsorbed oxygen contents on the surface of all samples decreased after thermal treatment, which may be caused by the large crystal size of aged samples, leading to the reduction of the surface oxygen vacancies.

### 3.3 Textural properties

Figure 4 shows the N<sub>2</sub> adsorption–desorption isotherms of CZLY-*X*-f and CZLY-*X*-a (*X*=20, 40, 60, 80), with the pore size distribution showing in the inserts in Figs. 4(a) and (b), respectively. The isotherms correspond to type IV with a type H2 hysteresis loop [15]. For CZLY-*X*-f (*X*=20, 40, 60,

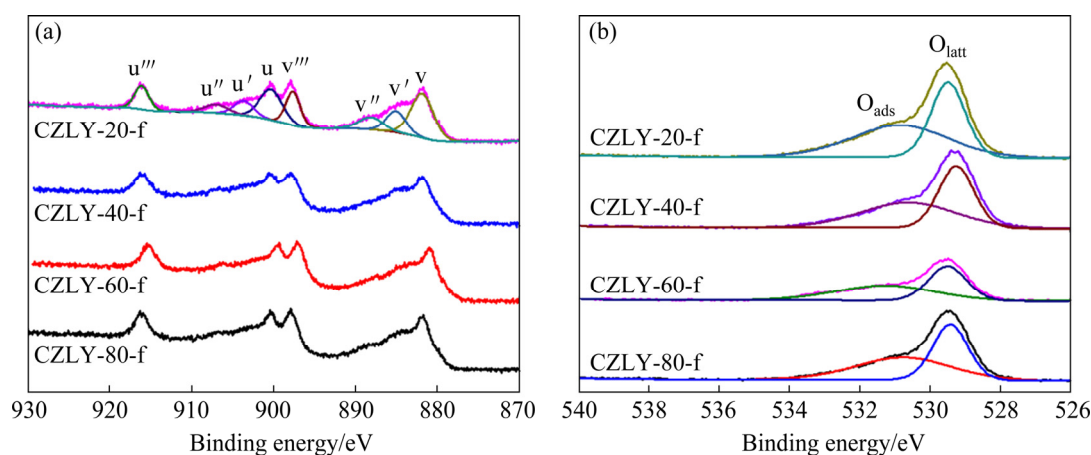
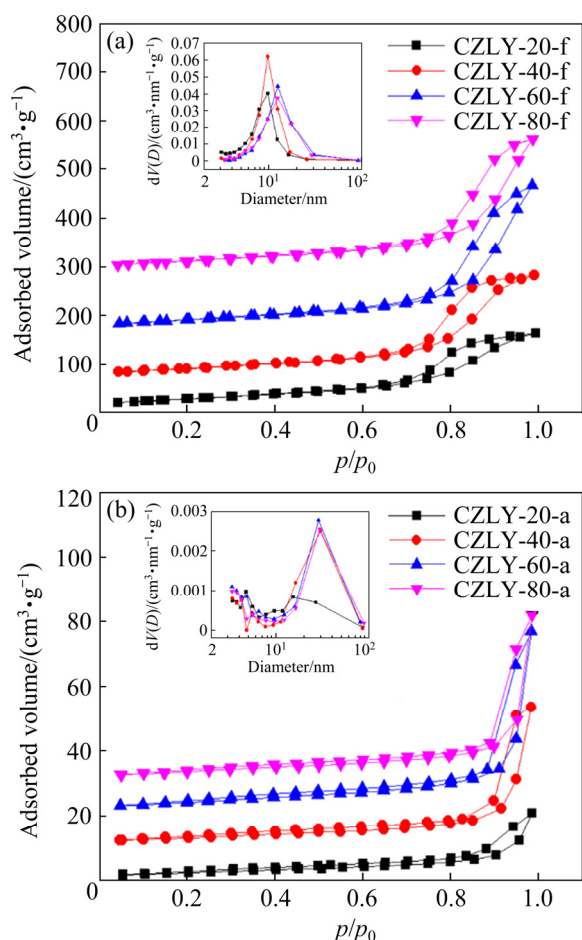


Fig. 3 XPS spectra of Ce 3d (a) and O 1s (b) for CZLY-*X*-f (*X*=20, 40, 60, 80) samples

Table 2 Surficial element compositions of CZLY-*X*-f and CZLY-*X*-a (*X*=20, 40, 60, 80)

Sample	Element composition/at.%			Ce <sup>3+</sup> /Ce molar ratio	O <sub>ads</sub> /O <sub>latt</sub> molar ratio
	Ce	Zr	La + Y		
CZLY-20-f	29.610	55.850	14.540	0.226	1.178
CZLY-40-f	30.245	55.786	13.970	0.231	1.086
CZLY-60-f	30.332	54.909	14.760	0.258	1.134
CZLY-80-f	30.339	55.614	14.047	0.254	1.082
CZLY-20-a	17.992	53.479	28.529	0.176	0.985
CZLY-40-a	25.773	55.017	19.211	0.148	0.868
CZLY-60-a	24.905	55.333	19.762	0.158	0.930
CZLY-80-a	24.716	54.261	21.023	0.152	0.992



**Fig. 4** N<sub>2</sub> adsorption–desorption isotherms and pore size distribution (insert) of CZLY-*X*-f (a) and CZLY-*X*-a (b) (*X*=20, 40, 60, 80)

80), the pore size distribution is mainly in the range of 2–50 nm. With the increase of the co-precipitation temperature, the most probable aperture for fresh samples shifts to the large size. As the crystal sizes of CZLY-*X*-f (*X*=20, 40, 60, 80) increase, we consider that the large crystal size has a positive effect on the formation of large pores. When the co-precipitation temperature reaches 60 °C, the largest probable aperture is obtained. After thermal treatment, the pore size distribution of samples changes a lot and shifts to large sizes, which is due to the migration and sintering of crystal grains during calcination. It can be observed that the total pore volume and average pore diameter of the CZLY-20-a are the smallest, which may be explained by serious sintering because of small crystal size. As co-precipitation temperature increases, the average crystal size is enlarged, thus, the thermal stability of the sample is promoted. Notably, the pore size change of CZLY-60-a is the

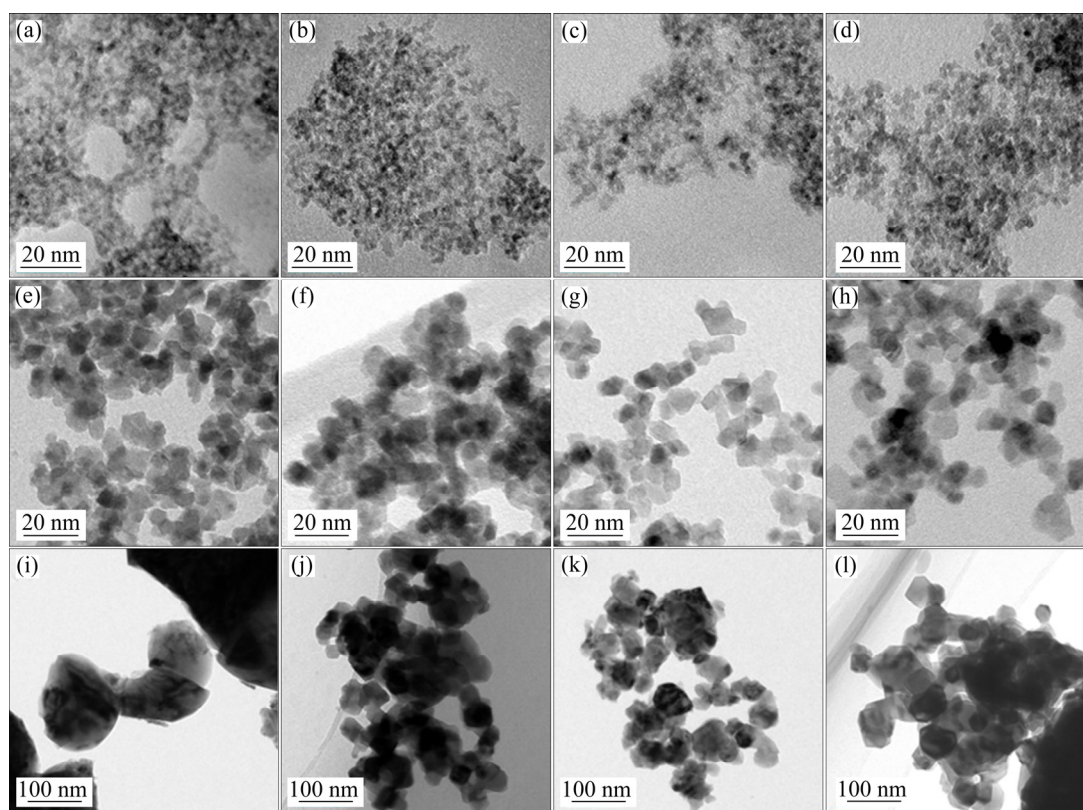
smallest among the aged samples, indicating its good thermal stability.

Table 3 shows the specific surface area ( $S_{\text{BET}}$ ), the total pore volume and the average pore diameter of CZLY-*X*-f and CZLY-*X*-a (*X*=20, 40, 60, 80). As seen, all CZLY-*X*-f (*X*=20, 40, 60, 80) have large specific surface area higher than 100 m<sup>2</sup>/g. When the co-precipitation temperature increases from 20 to 60 °C, the specific surface area of fresh samples increases from 102.24 (CZLY-20-f) to 112.12 m<sup>2</sup>/g (CZLY-60-f). The total pore volume and average pore size of CZLY-60-f are the largest, i.e. 0.48 cm<sup>3</sup>/g and 16.93 nm, respectively. Compared with CZLY-*X*-f (*X*=20, 40, 60, 80), the specific surface area and total pore volume of CZLY-*X*-a (*X*=20, 40, 60, 80) are decreased seriously, which is caused by the collapse of pore structure and the sintering of the particles after thermal treatment. Among all aged samples, CZLY-60-a has the largest specific surface area of 15.42 m<sup>2</sup>/g and the largest total pore volume of 0.09 cm<sup>3</sup>/g. As described in Ref. [15], the accumulation state and size of crystal grains impact the thermal stability of CZs. Thus, it is concluded that the large crystal size and long migration distance of grains of CZLY-60-f are responsible for its high thermal stability.

**Table 3** Specific surface areas and pore structures of CZLY-*X*-f and CZLY-*X*-a (*X*=20, 40, 60, 80)

Sample	$S_{\text{BET}}/$ (m <sup>2</sup> ·g <sup>-1</sup> )	Total pore volume/(cm <sup>3</sup> ·g <sup>-1</sup> )	Average pore diameter/nm
CZLY-20-f	102.24	0.25	9.88
CZLY-40-f	109.33	0.34	12.59
CZLY-60-f	112.12	0.48	16.93
CZLY-80-f	111.35	0.44	15.65
CZLY-20-a	8.92	0.03	14.38
CZLY-40-a	11.58	0.07	23.17
CZLY-60-a	15.42	0.09	22.80
CZLY-80-a	13.25	0.08	24.26

Figure 5 shows the TEM images of CZLY-*X*-d, CZLY-*X*-f and CZLY-*X*-a (*X*=20, 40, 60, 80). As seen, the CZLY-*X*-d (*X*=20, 40, 60, 80) are composed of crystals with a size in the range of 2–5 nm, which have low crystallinity and indistinct grain boundaries. The CZLY-*X*-f (*X*=20, 40, 60, 80) are composed of many polyhedral crystals with a size in the range of 5–10 nm. With the co-precipitation temperature increasing from 20 to



**Fig. 5** TEM images of CZLY-20-d (a), CZLY-40-d (b), CZLY-60-d (c), CZLY-80-d (d), CZLY-20-f (e), CZLY-40-f (f), CZLY-60-f (g), CZLY-80-f (h), CZLY-20-a (i), CZLY-40-a (j), CZLY-60-a (k), and CZLY-80-a (l)

60 °C, the dispersion of grains of CZLY-*X*-f (*X*=20, 40, 60) is improved and the grain boundaries become clear. Further, a certain amount of crystal grains of CZLY-*X*-d and CZLY-*X*-f (*X*=20, 40, 60, 80) are selected for the statistics of crystal size, and the results are shown in Fig. 6. The average crystal sizes of CZLY-20-d, CZLY-40-d, CZLY-60-d and CZLY-80-d are 3.2, 3.4, 3.6, and 3.4 nm, respectively, demonstrating that properly increasing the co-precipitation temperature could promote the growth of grains. Meanwhile, the average crystal sizes of CZLY-*X*-f (*X*=20, 40, 60) show an increasing trend from 7.3 to 7.7 nm, which is consistent with the results of XRD. After thermal treatment, the grains of CZLY-*X*-a (*X*=20, 40, 60, 80) become larger. As the crystal sizes of aged samples are too large and heterogenous, the crystal size distribution of CZLY-*X*-a (*X*=20, 40, 60, 80) is difficult to obtain due to agglomeration. CZLY-60-a has the smallest crystal size among the aged samples, revealing the best thermal stability.

### 3.4 Redox properties

Figure 7 shows the H<sub>2</sub>-TPR curves of

CZLY-*X*-f and CZLY-*X*-a (*X*=20, 40, 60, 80). All fresh samples display a broad reduction feature centered at 560 °C, which corresponds to the reduction of bulk Ce<sup>4+</sup> species [23]. After thermal treatment, the reduction temperature of bulk Ce<sup>4+</sup> increases, which is due to the structure deterioration and the collapse of pores caused by high temperature [24]. It should be noted that, the bulk Ce<sup>4+</sup> reduction temperature of CZLY-20-a increases from 560 to 830 °C, which can be attributed to the inhomogeneous element distribution and crystal particles sintering. As to CZLY-60-a, the bulk Ce<sup>4+</sup> reduction temperature only increases from 560 to 620 °C. This reveals that CZLY-60-a has good redox properties.

Figure 8 shows the OSC values of CZLY-*X*-f and CZLY-*X*-a (*X*=20, 40, 60, 80). For CZLY-*X*-f (*X*=20, 40, 60, 80), the OSC values of CZLY-40-f, CZLY-60-f and CZLY-80-f are all higher than 490.0 μmol/g. However, the OSC value of CZLY-20-f is lower than 400.0 μmol/g. This may be attributed to the low content of active Ce element and surficial Ce<sup>3+</sup> species. Among the aged samples, the OSC value of CZLY-20-a is also the smallest,

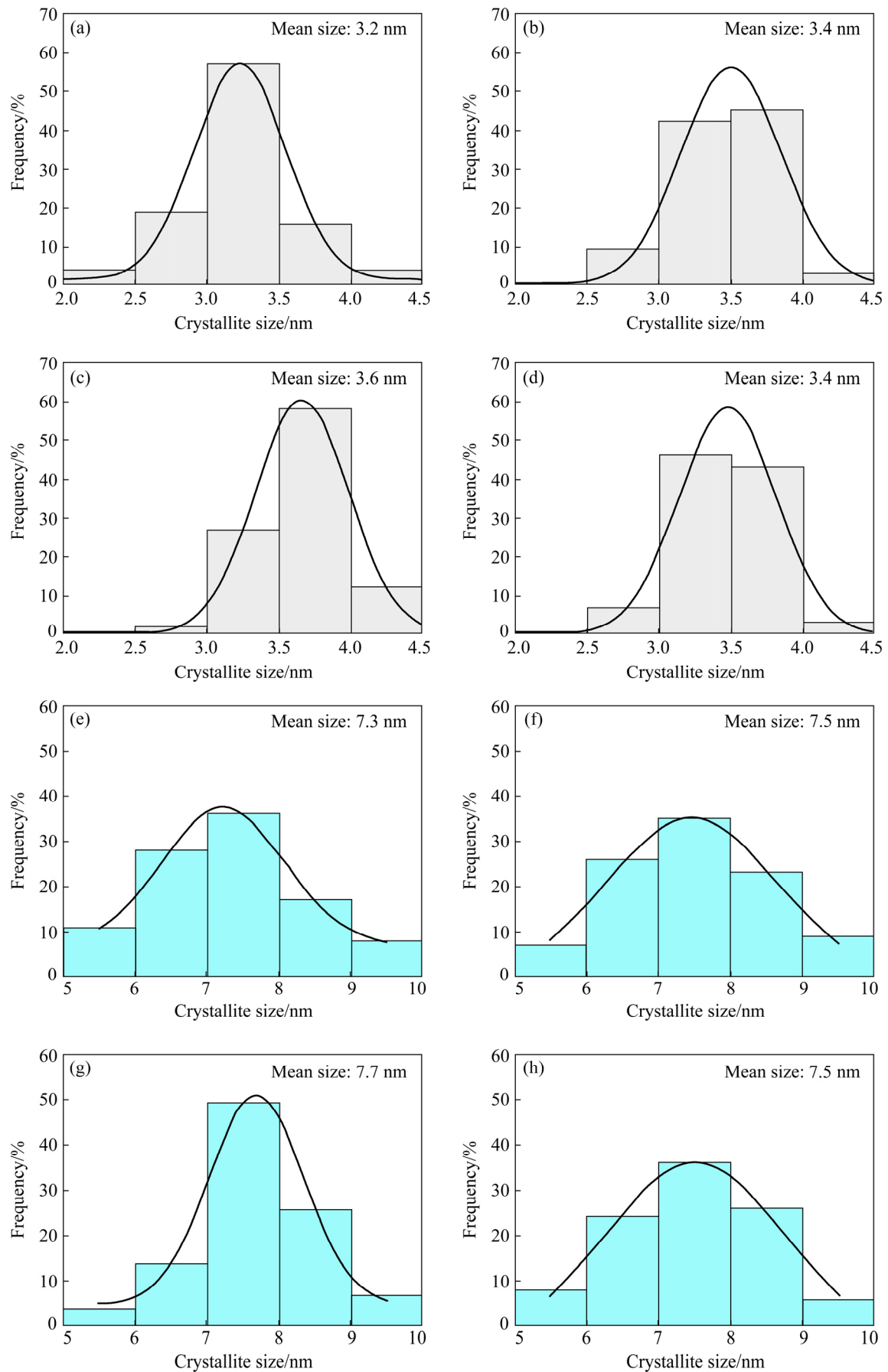


**Fig. 6** Crystal size distribution statistics of CZLY-20-d (a), CZLY-40-d (b), CZLY-60-d (c), CZLY-80-d (d), CZLY-20-f (e), CZLY-40-f (f), CZLY-60-f (g), and CZLY-80-f (h)

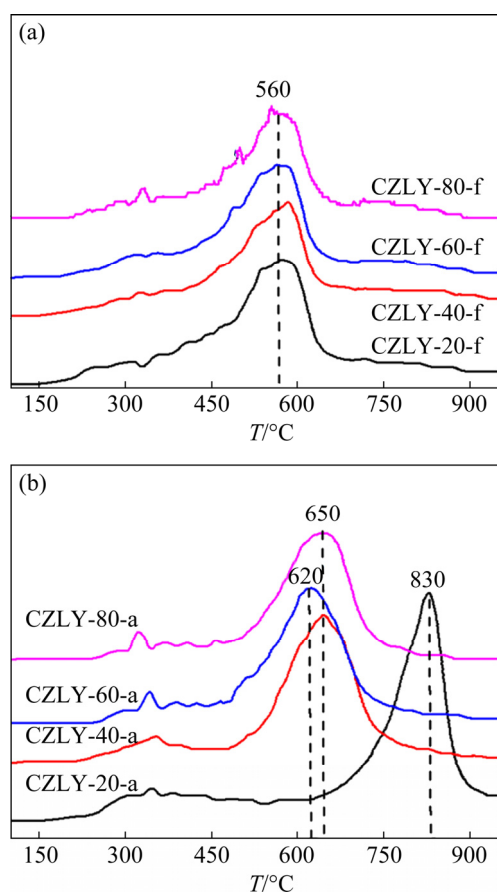


**Fig. 7** H<sub>2</sub>-TPR curves of CZLY-*X*-f (a) and CZLY-*X*-a (b) (*X*=20, 40, 60, 80)

which can be explained by the serious sintering of particles and the rearrangement of element. When the co-precipitation temperature is higher than 20 °C, the OSC values of CZLY-*X*-a (*X*=40, 60, 80) show little change, all of which are larger than 450.0 μmol/g, and CZLY-60-a has the highest OSC value of 497.7 μmol/g.

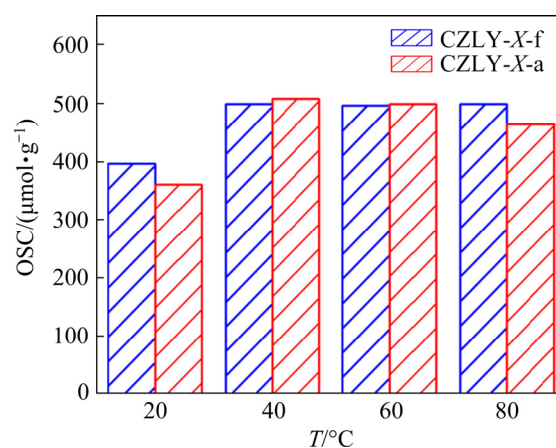


**Fig. 8** OSC values of CZLY-*X*-f and CZLY-*X*-a (*X*=20, 40, 60, 80)

### 3.5 Influencing mechanism of co-precipitation temperature on structure and properties of CZLYs

A mechanism that the co-precipitation temperature influences the structure and properties of CZLYs is proposed based on the above results. As an important reaction thermodynamic parameter, the co-precipitation temperature has significant effects on the viscosity of the system, the mass transfer rate, and the nucleation and growth of crystal grains [25,26]. The influencing mechanism of co-precipitation temperature on structure and properties of CZLYs [27] is shown in Fig. 9. When the co-precipitation temperature is low, the nucleation rate of crystal grains is faster than the growth rate, resulting in small-sized crystal grains. To reduce the high surface energy, the small crystal grains tend to assemble and accumulate, leading to poor thermal stability. On the other hand, the

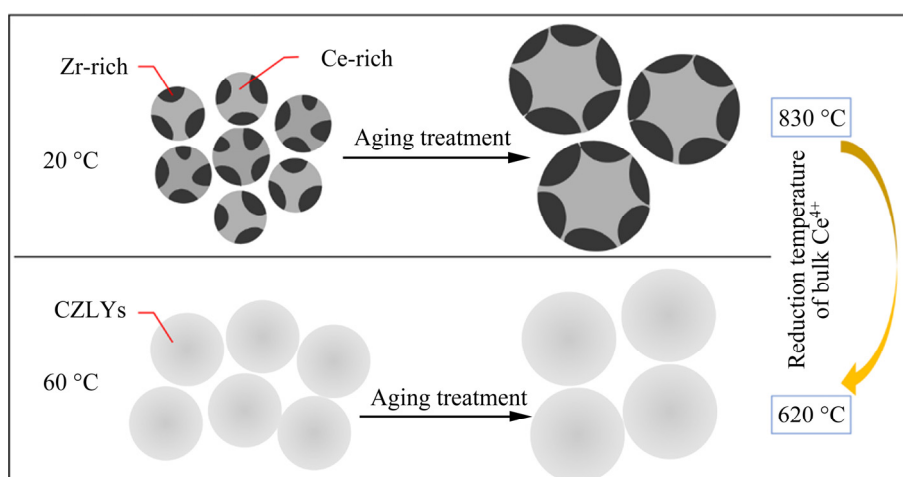


**Fig. 9** Influencing mechanism of co-precipitation temperature on structure and properties of CZLYs

microscopic homogeneity of the precursor is also unsatisfactory because of the low mass transfer rate at low co-precipitation temperature, which causes inhomogeneous element distribution of CZLYs, probably with Ce-rich and Zr-rich components. When the temperature of preparation system increases to a proper value, the increased growth rate promotes the growth of crystal grains, with the improved uniformity of the precursor because of the promoted mass transfer rate, leading to good element distribution of the samples [28]. However, continuing to increase the co-precipitation temperature may restrain the growth of crystal grains by promoting the nucleation rate larger than the growth rate [15]. In summary, a proper co-precipitation temperature is a necessary condition for obtaining CZLYs with good thermal stability and redox properties.

## 4 Conclusions

(1) A series of CZLYs with cubic phase structure were synthesized by co-precipitation method. After thermal treatment at 1100 °C for 10 h, the Ce element migrated from the surface to the bulk and the enrichment of La and Y elements on the surface happened. With the increase of co-precipitation temperature, the growth of grains is promoted, and the material has good dispersion and uniformity of grains, which leads to good thermal stability and redox properties.

(2) When the co-precipitation temperature is 60 °C, the prepared CZLY-60 material shows the best thermal stability and redox properties. After treatment at 1100 °C for 10 h, CZLY-60-a has the largest total specific surface area of 15.42 m<sup>2</sup>/g and the largest total pore volume of 0.09 cm<sup>3</sup>/g. Meanwhile, it also has the best redox property with the lowest bulk Ce<sup>4+</sup> reduction temperature of 620 °C and high OSC of 497.7 μmol/g.

## Acknowledgments

The authors are grateful for the financial supports from the Hebei Key Research and Development Program, China (No. 20374202D), and the Hebei High Level Talent Team Building, China (No. 205A1104H).

## References

[1] WU Ye, ZHANG Shao-jun, HAO Ji-ming, LIU Huan, WU

- Xiao-meng, HU Jing-nan, WALSH M P, WALLINGTON T J, ZHANG K M, STEVANOVIC S. On-road vehicle emissions and their control in China: A review and outlook [J]. *Science of the Total Environment*, 2017, 574: 332–349.
- [2] HE Jun-jun, WANG Cheng-xiong, ZHENG Ting-ting, ZHAO Yun-kun. Thermally induced deactivation and the corresponding strategies for improving durability in automotive three-way catalysts [J]. *Johnson Matthey Technology Review*, 2016, 60(3): 196–203.
- [3] ROOD S, ESLAVA S, MANIGRASSO A, BANNISTER C. Recent advances in gasoline three-way catalyst formulation: A review [J]. *Proceedings of the Institution of Mechanical Engineers (Part D): Journal of Automobile Engineering*, 2020, 234(4): 936–949.
- [4] DEVAIAH D, REDDY L H, PARK S E, REDDY B M. Ceria–zirconia mixed oxides: Synthetic methods and applications [J]. *Catalysis Reviews*, 2018, 60(2): 177–277.
- [5] LIU Ji-xing, ZHAO Zhen, XU Chun-ming, LIU Jian. Structure, synthesis, and catalytic properties of nanosize cerium–zirconium-based solid solutions in environmental catalysis [J]. *Chinese Journal of Catalysis*, 2019, 40(10): 1438–1487.
- [6] LUCIANI G, LANDI G, IMPARATO C, VITIELLO G, DEORSOLA F A, DI BENEDETTO A, ARONNE A. Improvement of splitting performance of Ce<sub>0.75</sub>Zr<sub>0.25</sub>O<sub>2</sub> material: Tuning bulk and surface properties by hydrothermal synthesis [J]. *International Journal of Hydrogen Energy*, 2019, 44(33): 17565–17577.
- [7] KSAPABUTR B, GULARI E, WONGKASEMJIT S. Sol-gel derived porous ceria powders using cerium glycolate complex as precursor [J]. *Materials Chemistry and Physics*, 2006, 99(2/3): 318–324.
- [8] WANG Man-juan, GU Ying-ying, QIN Li-ping, LI Jin-jin, XU Wen-yang. Synthesis of mesoporous cerium-zirconium mixed oxides by hydrothermal templating method [J]. *Journal of Central South University of Technology*, 2008, 15(6): 796–800.
- [9] MARTÍNEZ-ARIAS A, FERNÁNDEZ-GARCÍA M, BALLESTEROS V, SALAMANCA L N, CONESA J C, OTERO C, SORIA J. Characterization of high surface area Zr–Ce (1:1) mixed oxide prepared by a microemulsion method [J]. *American Chemical Society*, 1999, 15(14): 4796–4802.
- [10] WANG Qi, CUI Mei-sheng, HOU Yong-ke, ZHONG Qiang, YUE Mei, HUANG Xiao-wei. The effect of precipitation pH on thermal stability and structure of Ce<sub>0.35</sub>Zr<sub>0.55</sub>(LaPr)<sub>0.1</sub>O<sub>2</sub> oxides prepared by co-precipitation method [J]. *Journal of Alloys and Compounds*, 2017, 712: 431–436.
- [11] WU Yu-en, WANG Ding-sheng, LI Ya-dong. Understanding of the major reactions in solution synthesis of functional nanomaterials [J]. *Science China: Materials*, 2016, 59(11): 938–996.
- [12] WU Qing-feng, CUI Ya-juan, ZHANG Hai-long, ZHOU Yi, LAN Li, WANG Jian-li, CHEN Yao-qiang. Preparation of ceria–zirconia mixed oxides with improved thermal stability for three-way catalysts by a modified co-precipitation method [J]. *Journal of Inorganic Materials*, 2017, 32(3): 331–336.
- [13] YUE Mei, CUI Mei-sheng, ZHANG Na, LONG Zhi-qi, HUANG Xiao-wei. Characterization of CeO<sub>2</sub>–ZrO<sub>2</sub> mixed oxides prepared by two different co-precipitation methods [J].

- Journal of Rare Earths, 2013, 31(3): 251–256.
- [14] ZHOU Yi, XIONG Lei, DENG Jie, WANG Jian-li, YUAN Shan-dong, LAN Li, CHEN Yao-qiang. Facile synthesis of high surface area nanostructured ceria–zirconia–yttria–lanthana solid solutions with the assistance of lauric acid and dodecylamine [J]. Materials Research Bulletin, 2018, 99: 281–291.
- [15] CUI Ya-juan, FANG Rui-mei, SHANG Hong-yan, SHI Zhong-hua, GONG Man-chu, CHEN Yao-qiang. The influence of precipitation temperature on the properties of ceria–zirconia solid solution composites [J]. Journal of Alloys and Compounds, 2015, 628: 213–221.
- [16] RAHNAMA A, GHARAGOZLOU M. Preparation and properties of semiconductor CuO nanoparticles via a simple precipitation method at different reaction temperatures [J]. Optical and Quantum Electronics, 2012, 44(6/7): 313–322.
- [17] PALMERO P, ESNOUF C, MONTANARO L, FANTOZZI G. Influence of the co-precipitation temperature on phase evolution in yttrium–aluminium oxide materials [J]. Journal of the European Ceramic Society, 2005, 25(9): 1565–1573.
- [18] REDDY B M, LAKSHMANAN P, KHAN A, LÓPEZ-CARTES C, ROJAS T C, FERNÁNDEZ A. Structural characterization of CeO<sub>2</sub>–ZrO<sub>2</sub>/TiO<sub>2</sub> and V<sub>2</sub>O<sub>5</sub>/CeO<sub>2</sub>–ZrO<sub>2</sub>/TiO<sub>2</sub> mixed oxide catalysts by XRD, Raman spectroscopy, HREM, and other techniques [J]. The Journal of Physical Chemistry B, 2005, 109(5): 1781–1787.
- [19] NELSON A E, SCHULZ K H. Surface chemistry and microstructural analysis of Ce<sub>x</sub>Zr<sub>1-x</sub>O<sub>2-y</sub> model catalyst surfaces [J]. Applied Surface Science, 2003, 210(3/4): 206–221.
- [20] RICOTE S, JACOBS G, MILLING M, JI Ya-ying, PATTERSON M P, DAVIS B H. Low temperature water–gas shift: Characterization and testing of binary mixed oxides of ceria and zirconia promoted with Pt [J]. Applied Catalysis A: General, 2006, 303(1): 35–47.
- [21] ATRIBAK I, BUENO-LÓPEZ A, GARCÍA-GARCÍA A. Role of yttrium loading in the physico-chemical properties and soot combustion activity of ceria and ceria–zirconia catalysts [J]. Journal of Molecular Catalysis A: Chemical, 2009, 300(1/2): 103–110.
- [22] WANG Qi, YUE Mei, ZHONG Qiang, CUI Mei-sheng, HUANG Xiao-wei, HOU Yong-ke, WANG Lei, YANG Yu-xuan, LONG Zhi-qi, FENG Zong-yu. Structure and properties of cerium zirconium mixed oxide prepared under different precipitate aging processes [J]. Journal of Rare Earths, 2016, 34(7): 695–703.
- [23] KAMIUCHI N, HANEDA M, OZAWA M. Enhancement of OSC property of Zr rich ceria–zirconia by loading a small amount of platinum [J]. Catalysis Today, 2014, 232: 179–184.
- [24] FORNASIERO P, MONTINI T, GRAZIANI M, KAŠPAR J, HUNGRÍA A B, MARTÍNEZ-ARIAS A, CONESA J C. Effects of thermal pretreatment on the redox behaviour of Ce<sub>0.5</sub>Zr<sub>0.5</sub>O<sub>2</sub>: Isotopic and spectroscopic studies [J]. Physical Chemistry Chemical Physics, 2002, 4(1):149–159.
- [25] MULLIN J W. Crystallization [M]. 4th ed. Massachusetts: Reed Educational and Professional Publishing Ltd, 2001: 181–284.
- [26] PARK J, JOO J, KWON S, JANG Y, HYEON T. Synthesis of monodisperse spherical nanocrystals [J]. Angewandte Chemie, 2007, 46(25): 4630–4660.
- [27] MAMONTOV E, BREZNY R, KORANNE M, EGAMI T. Nanoscale heterogeneities and oxygen storage capacity of Ce<sub>0.5</sub>Zr<sub>0.5</sub>O<sub>2</sub> [J]. Journal of Physical Chemistry B, 2004, 35(6): 13007–13014.
- [28] QIU Guan-zhou, SONG Xiao-lan, QU Peng, YANG Zhen-hua, WU Xue-lan, WANG Hai-bo. Effect factors on synthesis of CeO<sub>2</sub> nanoparticle by precipitation method [J]. Journal of Rare Earths, 2005, 23(3): 321–327.

## 共沉淀温度对镧和钇掺杂的 铈锆复合氧化物结构和性能的影响

张连杰<sup>1,2</sup>, 崔梅生<sup>1,2,3,4</sup>, 王昊<sup>1,2,3</sup>, 侯永可<sup>1,2,3</sup>, 陈士磊<sup>1,2</sup>, 翟志哲<sup>1,3</sup>, 龙志奇<sup>1,2,3,4</sup>, 张永奇<sup>1,2,3,4</sup>

1. 有研科技集团有限公司 稀土国家工程研究中心, 北京 100088;
2. 北京有色金属研究总院, 北京 100088;
3. 有研稀土新材料股份有限公司, 北京 100088;
4. 有研稀土高技术有限公司, 廊坊 065201

**摘要:** 铈锆复合氧化物因具有储放氧的能力而被视为汽车三效催化剂中的关键材料。为了揭示共沉淀温度对多元掺杂铈锆复合氧化物的结构和理化性能的影响, 采用共沉淀法合成一系列镧和钇掺杂的铈锆复合氧化物, 并通过 XRD、N<sub>2</sub> 吸附脱附、TEM、XPS、储氧量(OSC)和 H<sub>2</sub> 程序升温还原(H<sub>2</sub>-TPR)等手段对 CZLYs 的理化性质进行系统表征。结果表明, 共沉淀温度是影响 CZLYs 晶粒尺寸、储氧性能和热稳定性的重要参数。共沉淀温度为 60 °C 时制备的样品具有最佳氧化还原能力和热稳定性, 经 1100 °C、10 h 高温热处理后得到的老化样品的比表面积和储氧量分别为 15.42 m<sup>2</sup>/g 和 497.7 μmol/g。此外, 还提出共沉淀温度对 CZLYs 结构和性能的影响机理。

**关键词:** 镧和钇掺杂; 铈锆复合氧化物; 共沉淀温度; 晶粒尺寸; 热稳定性